Article

Mapping Latent Heat Flux in the Western Forest Covered Regions of Algeria Using Remote Sensing Data and a Spatialized Model

Souidi Zahira [1,*], Hamimed Abderrahmane [1], Khalladi Mederbal [1] and Donze Frederic [2,3]

[1] Research on Biological Systems and Geomatics Laboratory, University of Mascara, P.O.Box 305, Mascara, 29000, Algeria; E-Mails: hamimed@dr.com (H.A.); kmederbal@hotmail.com (K.M.)

[2] 3S-R laboratory, University of Grenoble, BP 53 – 38041, Grenoble cedex 9, France

[3] QCAT, CSIRO, PO Box 883, Kenmore, QLD, 4069, Australia; E-Mail: frederic.donze@csiro.au

* Author to whom correspondence should be addressed; E-Mail: souidi.z@gmail.com;
Tel.: +213-45-812-640; Fax: +213-45-821-238.

Abstract: The present paper reports on an investigation to monitor the drought status in Algerian forest covered areas with satellite Earth observations because ground data are scarce and hard to collect. The main goal of this study is to map surface energy fluxes with remote sensing data, based on a simplified algorithm to solve the energy balance equation on each data pixel. Cultivated areas, forest cover and a large water surface were included in the investigated surfaces. The input parameters involve remotely sensed data in the visible, near infrared and thermal infrared. The surface energy fluxes are estimated by expressing the partitioning of energy available at the surface between the sensible heat flux (H) and the latent heat flux (LE) through the evaporative fraction (Λ) according to the S-SEBI (Simplified Surface Energy Balance Index) concept. The method is applicable under the assumptions of constant atmospheric conditions and sufficient wet and dry pixels over a Landsat 7 image. The results are analyzed and discussed considering instantaneous latent heat flux at the data acquisition time. The results confirm the relationships between albedo (r_0), the surface temperature (T_0) and the evaporative fraction. The method provides estimates of air temperature and LE close to reference measurements. The estimate of latent heat flux and other variables are comparable to those of previous studies. Their comparison with other methods shows reasonable agreement. This approach has demonstrated its simplicity and the fact that remote sensing data alone is sufficient; it could be very promising in areas where data are scarce and difficult to collect.

---

1. Introduction

Forest ecosystems as open systems are linked to the atmosphere and to the pedosphere by energy and matter fluxes. Functioning of the ecosystem manifests itself through these fluxes in space and time, which are controlled by the pertaining source and/or sink strengths of the ecosystem and, in case of interaction with the atmosphere, by convective and turbulent transport conditions. Water and energy flux rates are an expression of primary production processes and production rates in forest ecosystems. Depending on tree species, site conditions and tree health status, the quantification of latent and sensible heat flux is an important and valuable tool in forest ecosystem research, particularly for natural community drought assessment [1]. Vegetation water content is a key factor to evaluate fire susceptibility [2].

Indeed, the vegetation status is an indicator of the degree of stress experienced by plants in their environment [3]. Vegetation stress can be defined as any disturbance that adversely influences growth [4]. This stress can be due to many factors, one of which is water deficiency that restricts transpiration, inducing closure of stomata and resulting in less water evaporating from the leaf surface. Because less cooling occurs due to water evaporation, leaf temperature increases [4]. As an alternative to measuring the vegetation water content to assess short-term fire risk, Chuvieco *et al.* [5] investigated the possibility of using the thermal dynamic of vegetation. They assumed that differences between the air and surface temperatures were related to plant water content and to water stress. In line with this assumption, several indices have been proposed to estimate vegetation status based on evapotranspiration [6].

The partitioning of energy fluxes above ecosystems into sensible and latent heat determines atmosphere water vapor and heat content. A significant contribution of water input into such ecosystems originates from the deposition of cloud droplets (fog). The intercepted water may drip to lower layers of the canopy or the forest soil, or may re-evaporate into the atmosphere. This re-evaporation is associated with a large latent heat flux. Therefore, less energy is available for the sensible heat flux and the diurnal temperature variations are damped. Conceptually, the energy balance equation at the surface is:

$$\text{Rn} = G + H + LE \tag{1}$$

which expresses the partition of the net radiation *Rn* between soil heat flux *G*, sensible heat flux *H* and latent heat flux *LE* (corresponding to evaporation of bare soil and transpiration of vegetation canopy).

The model assumes that the net radiation flux density is allocated among the latent, sensible, and soil heat flux densities and that allocation of net radiation can provide information on evapotranspiration.

The soil heat flux *G* is usually low if compared with the other terms [7]. This term is often neglected, or it is set to a fixed proportion of the net radiation (for forest G = 0.1 Rn) [8]. However, calculation of the sensible heat flux is extremely important because it commonly consumes 50% of conifer forest net radiation [9]. Then H is given by:

$$H = \frac{\rho . Cp}{r_{ah}}(T_0 - T_a) \tag{2}$$

where ρ is the density of air, Cp is the specific heat of air, T_0 is the canopy or surface temperature, T_a is the air temperature and r_{ah} the aerodynamic resistance to the flux of sensible heat.

The latent heat flux can be expressed as:

$$LE = \frac{\rho . Cp}{\gamma} \times \frac{e_{sat}(T_0) - e_a}{r_{ah} + r_s} \tag{3}$$

where γ is the psychrometric constant, *rs* is the surface resistance to evaporation, e_a is the water vapour pressure at reference height (z_a) and $e_{sat}(T_o)$ is the saturated vapor pressure at surface temperature.

Currently, however, little is known about evapotranspiration and plant water status in Algerian forests; direct measurements are difficult to obtain because steep slopes where forest cover is dominant are present and these would require very expensive data acquisition. In addition, conventional techniques that use point measurements to estimate the components of energy balance are representative only of local scales and cannot be extended to large areas because of the heterogeneity of land surfaces and the dynamic nature of heat transfer processes.

With the advent of thermal infrared scanners, proper evaluation of spatial variability has become feasible. These data provide a synoptic view of surface temperatures, an advantage not afforded by point surface temperature measurements. Therefore, a much more accurate averaging of surface temperatures over a given area can be obtained using thermal imagery, thus reducing the number of necessary ground-based measurements [10–14]. In addition, remote sensing provides an accurate description of the various cover types using digital classification procedures. Thus, with remote sensing, the spatial variability of surface temperature and cover type in forest ecosystems can be accurately described especially when monitoring drought conditions [15,16] and natural ecosystems [17–19]. Different methods have been developed to derive surface fluxes from remote sensing observations.

The approaches vary from purely empirical to more complex ones, including residual methods and those that have their basis in the biophysical properties characterizing a two-dimensional T_s/VI (surface temperature/vegetation index) scatterplot domain derived from remote sensing observations [20]. This leads to the classical triangle or trapezoidal shape of the temperature/vegetation cover diagram [21–25] with it's ―cold" (unstressed) and ―warm" (stressed) edges. The trapezoid method is often used to derive a spatial pattern of instantaneous stress level for a given TIR/NDVI image [26].

Methods using remote sensing information to estimate heat exchange between land surface and atmosphere can be broadly divided in two categories: in the first one, the sensible heat flux is calculated and then the latent heat flux is obtained as the residual component of the energy balance equation; In the second, the relative evaporation is estimated by means of an index (e.g., the CropWater Stress Index) using a combination equation [27–30]. Although successful estimations of heat fluxes have been obtained over small-scale horizontal homogeneous surfaces [31–33], difficulties remain in estimations of partial canopies which are geometrically and thermally heterogeneous [34,35]. Classical remote sensing flux algorithms based on surface temperature measurements in combination with spatially constant surface meteorological parameters may be suitable for assessing the surface fluxes on a small scale, but they will fail for larger scales at which the surface meteorological

parameters are no longer constant, and the surface geometrical and thermal conditions are neither homogenous nor constant.

Amongst these methods, the S-SEBI model is used here: it is a model which requires very few inputs (albedo, NDVI and surface temperature maps) to derive evapotranspiration from the evaporative fraction. The evaporative fraction (Λ) is the ratio of the surface latent heat flux over the sum of the surface latent and sensible heat fluxes. A simple method to obtain Λ combines albedo (r_0) and the land surface temperature (T_0) [30,36,37]. Detailed descriptions of this method as well as its results can be found in [38]. S-SEBI [37] directly estimates the evaporative fraction, on a pixel basis by means of a contextual relationship between surface temperature and albedo. It has been applied to estimate the evaporative fraction for crops and natural vegetation at different spatial scales and assumes that atmospheric conditions remain relatively constant across the study region. It also requires enough wet and dry pixels in the scene for hydrological contrast. The S-SEBI concept was previously applied to Landsat images for the estimation of instantaneous fluxes adapted to semi-arid Mediterranean regions [37].
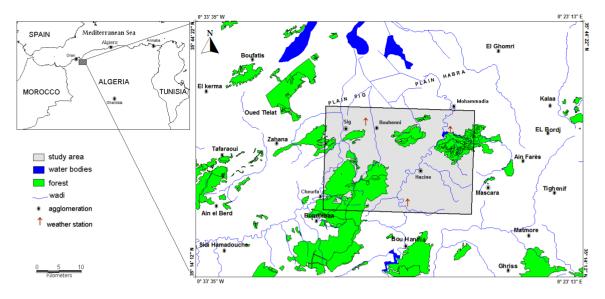
Landsat-7 ETM+ (Enhanced Thematic Mapper Plus) data were used to calculate the latent heat flux (LE). Landsat 7 is currently the sensor collecting multispectral thermal infrared data at high spatial resolution (60 m in TIR), which is very appropriate for model testing and direct ground comparison [39] although we have only three ground measurements in our study. In addition, it decreases the problem of pixel heterogeneity in the classification of vegetation. The ETM+ also includes additional features that make it a more versatile and efficient instrument for land cover monitoring and assessment [40].

The first objective of this study is to map surface energy fluxes with remote sensing data, based on a simplified algorithm to solve the energy balance equation for each pixel.

2. Site Description

The study site is located on the Mediterranean Sea in the western region of Algeria (Figure 1) over the mountains of Beni Chougrane, between longitudes 0°9' W and 0°6' E and latitude 35°21' N and 35°34' N. It covers an area of 742.5 km^2. Altitudes vary mostly in the range from 150 to 600 m, with a slope exceeding 25% on most of the land.
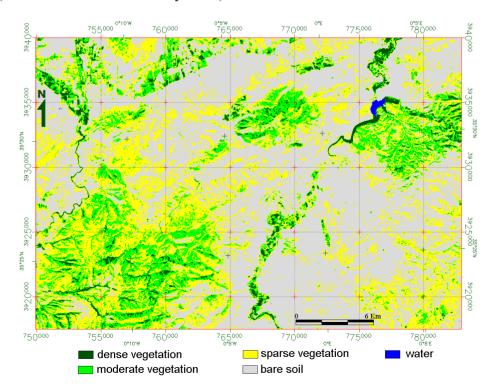
Two periods characterize this region: a cold season from November to April, with minimum recorded temperatures around 2 °C and a hot season from May to October with maxima of 35 °C. The maximum thermal stresses are worsened by the Sirocco, a hot drying wind from the south, which manifests itself especially in summer and increases evapotranspiration. Rainfall is concentrated during the cold season. The average annual rainfall is between 300 to 500 mm (data from 1970 to 2007 by NMO). The lithological faces which are widely represented in this region are marl and marl-limestone terrains with predominantly soft marls and clays [41].

Figure 1. Location of the study area.

The land cover map (Figure 2) shows that the soil use is diversified, but with a predominance of range and scrub (sparse vegetation) and forests (moderate vegetation) in the highland, as seen in the forest of Fergoug of Stamboul Bouziri which covers about 60% of the area under study. The forest vegetation is Mediterranean sclerophyllous evergreen, with three main vegetation types: a majority of *Thuya*, sparse pinery *(Pinus halepensis)* and loose areas of oak (*Quercus ilex*) [42]. The low vegetation is represented by *Calycotome*, *Diss*, *Chamerops*, *Artemesia* and *Stippa*. Down the mountain, lies the plain of Sig with irrigated crops and natural vegetation colonizing wadi beds (dense vegetation). Dry crops and fallow lands occupy most bare soils.

Figure 2. Land cover map of study area obtained by multispectral classification of TM image (Landsat-7 ETM+ at 29 May 2000).

This forest ecosystem is strategically important for the region's environmental (soil protection, carbon sequestration) and socioeconomic (tourism, timber harvest) systems. At present, the forests and their ecosystems are highly degraded, especially in summertime when trees die due water depletion, or are disease-prone and the forest is generally more susceptible to fire. While much attention is paid to Algerian forests, very few comprehensive studies have been done to address changes in this ecosystem at a regional scale.

3. Data Use and Input Parameters

The data set used in this study consists of seven spectral bands of Landsat-7 ETM+ (Enhanced Thematic Mapper Plus) sensor acquired on 29 May 2000 at 10:30 GMT. The solar conditions during the image acquisition of Landsat Thematic Mapper Plus on the selected day are reported in Table 1.

Table 1. Solar conditions during the image acquisition of Landsat Thematic Mapper on the selected day (day 150) in 2000.

Parameter	Unit	TM day 150
Solar declination	rad	0.3797
Sun-earth distance	AU	1.0138
Solar angle hour	rad	0.3938
Solar zenith angle	rad	0.4187

The estimation of the energy balance at the surface requires scanned spectral radiances under cloud free conditions in the visible, near-infrared and thermal infrared range to determine the input parameters: surface reflectance, surface temperature and vegetation index.

The spectral bands of ETM+ sensor are supplied in digit numbers (encoded into an 8-bit value) which are converted in radiances in the optical (visible, near and medium infrared) and thermal (thermal infrared) ranges using the linear expression:

$$L_\lambda = \alpha \cdot DN + \beta \tag{4}$$

where *DN* is the digit number, α and β are calibration coefficients.

The spectral radiances in the optical range are converted to reflectances after correction for atmospheric effects using MODTRAN radiative transfer code [43]. These reflectances are then used to calculate the albedo (r_0) and vegetation index (NDVI). The albedo is defined as a surface reflectance in the shortwave range (0.3–3 μm). It is calculated using the formula proposed by Liang *et al.* [44]:

$$r_0 = 0.356\, r_1 + 0.13\, r_3 + 0.373\, r_4 + 0.085\, r_5 + 0.072\, r_7 - 0.0018 \tag{5}$$

where r_1, r_3, r_4, r_5 and r_7 are respectively the reflectances in channels 1, 3, 4, 5 and 7 of ETM+ sensor. The vegetation index (NDVI) is calculated from the reflectances in the red (r_3) and the near infrared (r_4) [45]:

$$\mathrm{NDVI} = \frac{r_4 - r_3}{r_4 + r_3} \tag{6}$$

The spectral space-reaching radiance measured by the sensor in the thermal infrared ($L^{\uparrow}_{sat}(\lambda)$) is expressed by the following relationship [46]:

$$L^{\uparrow}_{sat}(\lambda) = [\varepsilon_{\lambda} L_{\lambda}(T_0) + (1 - \varepsilon_{\lambda}) L^{\downarrow}_{atm}(\lambda)]\tau_{\lambda} + L^{\uparrow}_{atm}(\lambda) \tag{7}$$

where $L_{\lambda}(T_0)$ is the radiance of a blackbody target of kinetic temperature T_0, τ_{λ} is the atmospheric transmission, $L^{\downarrow}_{atm}(\lambda)$ is the down-welling or sky radiance, $L^{\uparrow}_{atm}(\lambda)$ is the upwelling or atmospheric path radiance and ε_{λ} the emissivity of the surface which is estimated from the vegetation index (NDVI) [47]:

$$\varepsilon_{\lambda} = 1.0094 + 0.047 \log(NDVI) \tag{8}$$

The atmospheric parameters are estimated at time of satellite overpass by the web atmospheric correction parameters calculator [48]. Spectral radiances reflected from the Earth surface can be deduced by inversion of Equation 7. Surface temperatures are finally obtained based on these radiances according to Planck's Law [49]:

$$T_0 = \frac{1282.72}{\log(\dfrac{666.09}{L_{\lambda}(T_0)} + 1)} \tag{9}$$

Remote sensing data are supplemented by meteorological measurements for temperature and humidity of air, wind speed, global radiation and relative sunshine duration. These measurements are collected from three weather stations (Fergoug, Hacine and Bouhenni) located in the study area.

4. Methodology for Estimating Latent Heat Flux

The energy balance at the surface is determined with the Simplified Surface Energy Balance Index (S-SEBI) which is a simplified method, developed by Roerink *et al.* [37], to estimate surface fluxes. The derivation of accurate surface parameters from remote sensing is key to determine the main terms of energy balance depending on the type of vegetation in this model. With the model which combines surface parameters (input data) derived from remote sensing data with surface meteorological variables and vegetation characteristics, ET on local, regional and global-scales can be evaluated. Remote sensing information can provide spatial distribution and temporal evolution of NDVI (Normalized Difference Vegetation Index), surface albedo from visible and near-infrared bands and surface emissivity and radiometric surface temperature from mid and thermal infrared bands, which are indispensable to the model that partition the available energy into sensible and latent flux components [50]. However, eventhough the NDVI and albedo, provide interesting information to interpret thermal data [51], they are less significant in the discrimination of surface water status because their correlation coefficients with the latent heat flux are high. S-SEBI is based on the contrast between a reflectance (albedo) dependent maximum surface temperature for dry limit and a reflectance (albedo) dependent minimum surface temperature for a wet limit to discriminate between the available energy for sensible and latent heat fluxes. Since the atmospheric conditions over the study area can be regarded as constant and sufficient variations in surface hydrological conditions are present, the turbulent fluxes can then be calculated with S-SEBI without any further information than the remote sensing image itself [52].

In this model, the surface energy balance is obtained with remote sensing techniques on a pixel-by-pixel basis according to the following equation:

$$LE = \mathrm{Rn} - H - G \tag{10}$$

First, the surface net radiation (*Rn*) which represents the total heat energy that is partitioned into *G*, *H* and *LE*, is calculated according to:

$$\mathrm{Rn} = (1-r_0)\cdot Rg + L_\downarrow - L_\uparrow \tag{11}$$

where *Rg* measured at a weather station is the incoming global radiation ($Rg = K_{\downarrow exo}\tau_{sw}$) obtained from exo-atmospheric solar radiation $K_{\downarrow exo}$ taking into account the atmosphere transmissivity τ_{sw}. However, for sloping surfaces, *Rg* must be corrected pixel by pixel, using the surface slope and aspect information derived from a digital elevation model and the equation from Duffie and Beckman [53]. $L_\uparrow$ is the upwelling longwave radiation from the Stephan-Boltzman law [28] using surface temperature for a supposed emissivity of 1; $L_\downarrow$ is the downwelling longwave radiation using air temperature (Ta), vapor pressure (e_a) and atmosphere emissivity (ε'). It can be given by the following [54]:

$$\varepsilon' = 1.24\left(\frac{e_a}{T_a}\right)^{1/7} \tag{12}$$

Secondly, the soil heat flux cannot be directly determined from satellite sensors and requires an empirical formulation. The soil heat flux (*G*) has been estimated using the following relation developed by Bastiaanssen [28]:

$$\frac{G}{\mathrm{Rn}} = T_0(0.0038 + 0.0074\,r_0)\times\left(1 - 0.98\mathrm{NDVI}^4\right) \tag{13}$$

Thirdly, the sensible and latent heat fluxes are not calculated as separate parameters (see Equations 2 and 3) but from the evaporative fraction. In S-SEBI, the evaporative fraction is bounded by the dry and wet limits (Figure 3) and formulated by interpolating the reflectance (albedo) dependent surface temperature between the reflectance (albedo) dependent maximum surface temperature and the reflectance (albedo) dependent minimum surface temperature, which can be expressed as:

$$\Lambda = \frac{T_H - T_0}{T_H - T_{LE}} \tag{14}$$

where T_H corresponds to the minimum latent heat flux ($LE_{dry} = 0$) and maximum sensible heat flux ($H_{dry} = \mathrm{Rn} - G$) [the upper decreasing envelope when T_0 is plotted against surface reflectance (albedo)], T_{LE} is indicative of the maximum latent heat flux ($LE_{wet} = \mathrm{Rn} - G$) and minimum sensible heat flux ($H_{wet} = 0$) (the lower increasing envelope when T_0 is plotted against surface reflectance). A linear regression is applied to obtain T_H and T_{LE} from the surface reflectance (albedo):
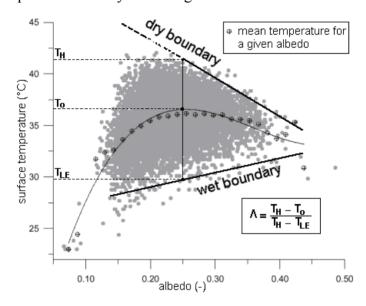
$$T_H = a_H + b_H \cdot r_0 \tag{15}$$

$$T_{LE} = a_{LE} + b_{LE} \cdot r_0 \tag{16}$$

where a_H, b_H, a_{LE} and b_{LE} are empirical coefficients estimated from the scatter plot of T_0 and r_0 in our study area.

Inserting Equations (15–16) into Equation (14), Λ can be derived by:

$$\Lambda = \frac{a_H + b_H \cdot r_0 - T_0}{a_H - a_{LE} + \left(b_H - b_{LE}\right) \cdot r_0} \tag{17}$$

Figure 3. Linear interpolation scheme to obtain evaporative fraction from albedo-surface temperature scatter plot in this study according to S-SEBI model.

Experimental evidence indicates that for homogeneous and heterogeneous land surfaces, Λ, is temporarily stable between 10:00 and 15:00 local time [55–57]. The evaporative fraction has therefore been selected as a basis to validate the instantaneous surface energy balance, which is expressed as [55]:

$$\Lambda = \frac{LE}{LE + H} = \frac{LE}{Rn - G} \tag{18}$$

The method furthermore assumes that:

$$H = (1 - \Lambda) \cdot (Rn - G) \tag{19}$$

$$LE = \Lambda(Rn - G) \tag{20}$$

In addition, the other parameters that are estimated are r_{ah}, r_s, and T_a. The r_{ah} value to study area is obtained by the inversion of Equation 2 and T_a is derived by linearly relating T_0 to the surface-air temperature difference [28]. r_s is obtained by the inversion of Equation 3. These parameters are not necessary to estimate the latent heat flux in the S-SEBI model, but it was added to refine the study and to assess the approach used.

5. Results and Discussion

5.1. Results Obtained with S-SEBI Method

It can be seen that the surface temperature is the most dominant parameter in the estimation of latent heat flux. Indeed, the S (of Simplified) in the S-SEBI model stands for the case where the extreme

temperatures T_{LE} and T_H can be determined from the image itself. In the study area, the surface temperature varies in the satellite image between 298.7 K minimum and 333.4 K maximum. A relatively higher average value is observed for dry pixels in comparison with wet pixels (Table 2). The higher values correspond to pixels where bare soils are dominant, while low values are associated with water or dense vegetation. The results are consistent with those obtained in Spain with the same method, where T_0 varies between 287 and 308 K [58].

Table 2. Instantaneous parameters and surface energy fluxes above dry and wet pixels estimated from remote sensing data and S-SEBI method.

Parameter	Unit	Dry pixels	Wet pixels
NDVI	–	0.117	−0.084
Albedo	–	0.310	0.120
Surface temperature	K	325.9	300.8
Emissivity	–	0.926	1.00
Net radiation	$W{\cdot}m^{-2}$	597.6	713.5
Soil heat flux	$W{\cdot}m^{-2}$	140.9	57.4
Sensible heat flux	$W{\cdot}m^{-2}$	466.6	0.0
Latent heat flux	$W{\cdot}m^{-2}$	0.0	656.1
Evaporation Fraction	–	0.0	1.0
Near-surface air temperature	K	295.9	275.2
Aerodynamic resistance to heat	$s{\cdot}m^{-1}$	58.7	223.4
Surface resistance to evaporation	$s{\cdot}m^{-1}$	3990.6	0.0

The aerodynamic resistance to sensible heat flux has a major influence on the latent heat density calculated for a given pixel; in this study it is only derived. The value of r_{ah} for dry pixels is low, causing the release of sensible heat to the atmosphere. This is justified by high differences between surface and air temperatures. The excess resistance parameter was larger over wet pixel, because the available energy at the surface is mainly used in evapotranspiration. The wet pixel is representative of the bare soil when the surface temperature was very close to the air temperature. The change of r_{ah} values implies a change in the relative verticalposition of the effective heat source (z_{0h}) and of the effective momentum sink (z_{0m}) within the canopy. More precisely a low value of r_{ah} implies that the heat source is higher than or very close to, the momentum sink. This is likely to happen when the upper portion of the canopy is warmer than the lower one. Indications that this might really be the case have been given by Jia [59], who studied in detail the variability within the canopy of radiative and convective fluxes in relation with foliage and soil temperature.

In comparison, with the resistance offered by the boundary layer to evaporation, the resistance offered by stomata (r_s) is generally larger in dry pixel (Table 2), but in still conditions r_{ah} can dominate the total external (i.e., r_{ah} plus r_s) leaf resistance. At the point of stomatal resistance to evaporation, the dry air increases in the atmosphere and the plant water status decreases.

Figure 4 shows the image illustrating the spatial variations of the latent heat flux derived by the S-SEBI procedures. All the methods indicate that the heat flux from the land surface varies significantly from place to place. The larger values (600–700 $W{\cdot}m^{-2}$) are obtained for water (blue on the image) and (400–300 $W{\cdot}m^{-2}$) evergreen forests (green on the image), intermediate (250–200 $W{\cdot}m^{-2}$) for sparse vegetation fields (yellow and orange) and the lowest for bare soil (red). These results are in

agreement with what we know about phenological stages for the various vegetation species in the area. These results represent the estimation of instantaneous LE (residual method); the simulations refer to a single snapshot taken at 10:30 AM. At midday it is a good indicator of the plant water status which is the basis of this study. For estimation of LE over longer periods (seasonal, monthly, daily estimations), the use of ground-based ET from weather data is necessary to make temporal interpolation. Therefore, temporal scaling, which is one of the weaknesses of remotely sensed data, is needed to convert the instantaneously spatial LE to a longer-time value (daily).
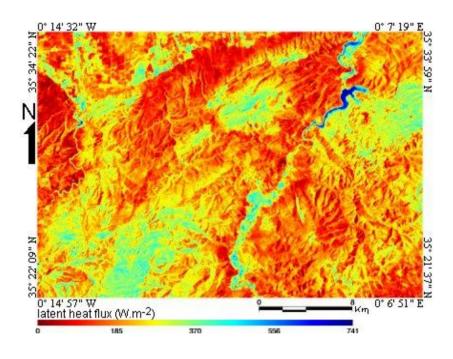
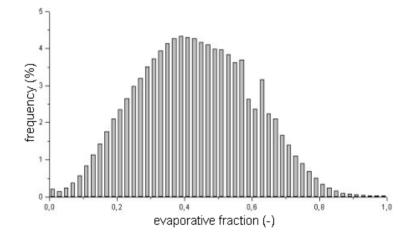**Figure 4.** Latent heat flux map.

Table 3 summarizes the surface energy fluxes and other indicators of different land cover units. The soil heat flux represents only 0.16 of the net radiation for the forest. Our results are comparable with those of Desbois *et al.* [8], where G measured over French forests represents 0.1 Rn. We can see that turbulent fluxes of sensible and latent heat play important role in the energy balance. They reach peak values that are about half the flux of solar radiation during a clear day. The amount of the flux of sensible heat is larger than the latent heat flux with lower wind speed (3 $s \cdot m^{-1}$). Apparently neither the sensible nor the latent heat flux is dominant over the other. Overall, the sensible heat flux averages to 258.69 $W \cdot m^{-2}$ and the latent heat flux is 249 $W \cdot m^{-2}$, which is about 41.74% and 40.18% of the net radiation balance, respectively. This is in good agreement with the result given by Jaeger *et al.* [60] of 250 $W \cdot m^{-2}$ latent heat flux measured for Mediterranean forests. The Bowen ratio (sensible/latent) has a higher value for forest vegetation in comparison with sparse vegetation (high albedo) of 1.4 and 0.8 respectively. Indeed, when the vegetation density increases, the sensible heat flux decreases. In contrast with the bare soil, the dense vegetation (wadi vegetation) has relatively higher values, usually on the order of 400 $W \cdot m^{-2}$. The sparse vegetation has very low values, usually less than 200 $W \cdot m^{-2}$. This can be explained by Mediterranean vegetation which is representative of the land cover of this region. This vegetation is mostly sparse and much degraded by overgrazing, which cannot maintain an

adequate soil moisture despite previous rainfalls (11.4 mm on 25 May 2000). This is because runoff rather than infiltration occurs in such soil and in this unfavorable regional topography.

Table 3. Variation of surface energy fluxes and moisture indicators with land cover units.

Land use	Rn(W·m^{-2})	G$_0$(W·m^{-2})	H(W·m^{-2})	LE(W·m^{-2})	Λ(−)
Water	745.91	64.48	23.17	658.25	0.96
Dense vegetation	650.09	92.78	164.15	393.15	0.71
Moderate vegetation	636.57	105.41	222.82	308.33	0.58
Sparse vegetation	618.56	115.91	279.67	222.97	0.44
Urban and bare soil	583.18	119.61	296.86	166.69	0.36

As shown from Table 3 the contribution of air humidity is important by the water bodies with a value of evaporation fraction approximately equal to 1. A decrease in the fraction of evaporation (Λ = 0.58) is observed for moderate vegetation forests even during the wet period of the year. Sparse vegetation although perennial is moderately dry (Λ = 0.4) with a significant portion of its energy converted into the sensible heat flux. The model notes the increase in the canopy-air temperature difference resulting in a greater net radiation being allocated to the sensible heat flux. This leaves less energy for the latent heat flux.

The results for the area understudy clearly show a small fraction of evaporation and a decrease in the latent heat flux in forest environments. This will have a direct impact on soil moisture and the drying up of vegetation which will be more pronounced in summer [61].The study area is marked with a dominance of moderately dry surfaces (0.3 < Λ <0.5) with a low LE (Figure 5).

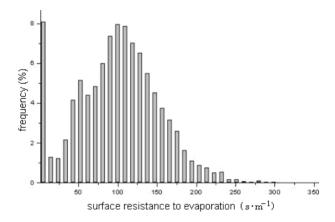**Figure 5.** Frequency distributions of evaporative fraction.

5.2. Evaluation Method

With this approach areas which have an increasing evaporation and those that suffer from water stress can be well differentiated at a regional scale. We see, from these observations that the fraction of evaporation and latent heat flux are direct and simple indicators to monitor drought conditions of natural environments. Sobrino *et al.* [50] used the S-SEBI model with AVHRR data acquired from 1997 to 2002 over the Iberian Peninsula to analyze the seasonal evolution of daily ET and a RMSE of 1.4 mm/d has been shown when results derived from S-SEBI were checked against with high

resolution ET values. Others works based on the S-SEBI method give realistic results [51]. In addition, the S-SEBI is not only simple but accurate when retrieving evapotranspiration data [58].
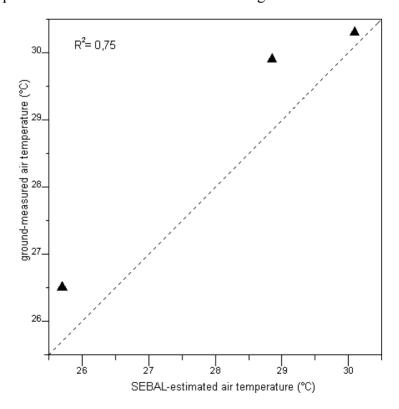
Therefore, the analysis of the frequency distribution of surface resistance to evaporation is considered a good way to validate our results. Bougeault *et al.* [62] and Bastiaanssen *et al.* [63] showed that for most surfaces fully covered by vegetation, the values of this resistance vary between 10 and 400 s·m^{-1}, with a peak usually around 80 s·m^{-1}. The result shown in Figure 6 is approximately consistent with this indication.

Figure 6. Frequency distribution of the canopy structure resistance to evaporation for pixels withNDVI values greater than 0.6.
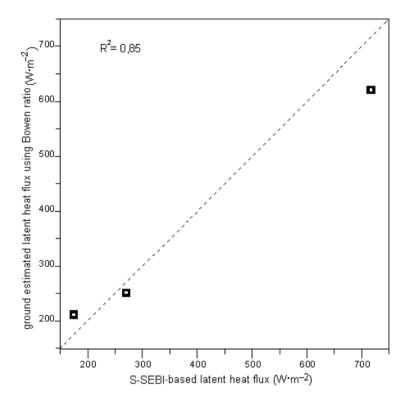

In addition, comparing the air temperature measured at three weather stations in our study area with those simulated by the model S-SEBI (Figure 7) a good fit (R^2 = 0.75) is found with a low root mean square error and with RMSE of only 0.78 °C of the observed Ta.

Figure 7. Comparison between the S-SEBI-based and ground-measured air temperatures.

We have compared our results with those estimated on the ground using the Bowen ratio [64]. To estimate the latent heat flux with the Bowen ratio method, measurements from weather stations in the study area of, Rn, G, Ta and e (vapor pressure) at two levels are used. The result of this comparison is shown in Figure 8. A sufficient correlation ($R^2 = 0.85$), with an RMSE of 64 $W \cdot m^{-2}$ of the Bowen ratio LE is seen.

Figure 8. Comparison between the ground-based and satellite-derived estimates of the latent heat flux.
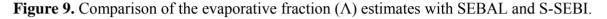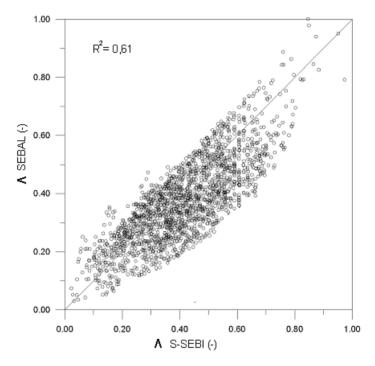

Another comparison is made using the SEBAL model [28] which is also based on the evaporative fraction in a manner similar to that of the S-SEBI model. When the evaporative fraction values obtained by SEBAL are compared with those estimated by S-SEBI (Figure 9) a reasonable fit ($R^2 = 0.61$) is obtained. However, when SEBAL is applied over mountainous areas as in the study area, adjustments based on a digital elevation model need to be made to T_0 and u (speed of the wind) to account for the lapse rate. Note that, errors in the surface temperatures or surface-air temperature differences have a great impact on the estimation of H. This is why we have different values at the same pixel from both methods. But the similarity between the SEBAL and S-SEBI results had already been verified by Weligepolage [65], who observed strong correlations between both algorithms, presenting a determination coefficient (R^2) of 0.95.

Another method can also be used to validate these results; the latent heat flux values obtained by S-SEBI and values estimated with the Priestley-Taylor formulation proposed by Jiang and Islam [66–67] are compared. This method is based on the interpretations of the remotely sensed T_0-NDVI triangle feature space, which can be expressed as:
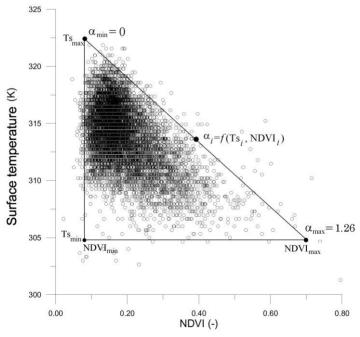
$$LE = \alpha \frac{\Delta}{\Delta + \gamma}(R_n - G) \tag{21}$$

where Δ is slope of the saturation vapor pressure-temperature relationship, γ is the psychrometric constant (0.66 mbK^{-1}) and α is the Priestley-Taylor parameter ranges from 0 to 1.26 (Figure 9). Two-step linear interpolation scheme [66,68,69] is used to get the value of α in Equation 21 based on the *Ts-NDVI* triangle feature space as shown in Figure 10. The other terms can be calculated using remotely sensed data [66].

Figure 9. Comparison of the evaporative fraction (Λ) estimates with SEBAL and S-SEBI.
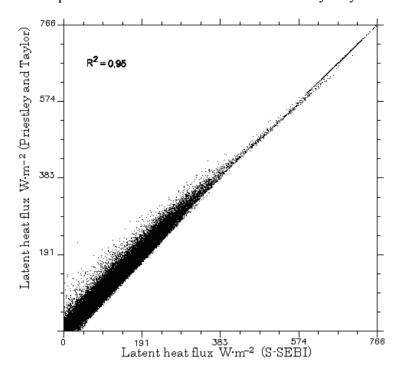

Figure 10. The simplified ND\VI-T_0 triangular space in the study area.

The confrontation of latent flux values obtained with the S-SEBI and Priestley-Taylor method shows that they are in good agreement (Figure 11), which justifies using this approach.

Figure 11. Comparison between the S-SEBI and Priestley-Taylor latent flux.

5.3. Sensitivity Analysis

The land surface temperature is the direct indicator of how much energy and water could be available over the land surface, as well as a key factor affecting the accuracy of the LE estimates. Land surface temperatures along with other related remotely sensed surface variables (input parameters) such as the surface albedo, the emissivity and NDVI in the energy balance models greatly contribute to the precise partitioning of the four energy components in these models and consequently to the accuracy of the retrieved regional LE.

In this work, the emissivity values estimated are reasonable according to reported values for soil and vegetation [47]. Given the pixel size (30 m), the differentiation of pixels is easier, leading to a more accurate NDVI estimation. Error for albedo is often lower. In Sobrino *et al.* [58] error estimates of 0.03 are found. To get accurate surface temperatures, atmospheric corrections and surface emissivity are used.

The uncertainty associated with the derived latent heat flux is large, because the evaporative fraction is determined solely by the surface temperature. If the surface temperature has large uncertainties, the resultant latent heat flux and evaporative fraction will be affected. In the S-SEBI formulation, this uncertainty is limited by consideration of the energy balance at the limiting cases (dry and wet).

However, the estimation of the instantaneous evaporative fraction error is the critical point of the sensitivity analysis. This is due to the fact that T_H and T_{LE} are obtained from a graphical procedure (see Figure 3) which may generate significant errors. In this context, a quantitative error estimation of Equation 14 is not easy. These errors are evaluated by Gómez *et al.* [70], who considered that the slopes of T_H and T_{LE} can reach an error of 15% and 70%, respectively, and the evaporative fraction can be obtained with an error of 20% approximately. It is clearly shown that in an ideal situation, T_H and T_{LE} must be obtained without error.

On the other hand, errors in net radiation estimations may be related to the errors in albedo estimations. Kustas and Norman [29] reviewed the uncertainties of various methods of estimating the net shortwave and long-wave radiation fluxes and found that a variety of remote sensing methods of surface net radiation estimation had an uncertainty of 5%–10% compared with ground-based observations on meteorological temporal scales. Since S-SEBI first calculates the net radiation balance and then partitions it into the energy balance terms, large discrepancies between the net radiation measurements and the measured energy balance closure values can be found. The S-SEBI calculated heat fluxes are systematically higher than the measured values in Roerink [37].

Moreover, in semiarid areas with sparse vegetation cover, errors in energy fluxes tend to be even higher, around 25% [71]. According to Roerink [37], all S-SEBI calculated values match the measured values within the measurement accuracy of approximately 10% [37].

Indeed, results from Roerink *et al.* [37], have shown that measured and estimated evaporative fraction values had a maximum relative difference of 8% when measurements obtained from a small field campaign during 1997 in Italy were compared with the S-SEBI derived outputs. Accuracy for the daily evapotranspiration using the S-SEBI method was found to be lower than 1 mm/d over a barrax test site in the framework of the DAISEX (Digital Airborne Imaging Spectrometer Experiment) campaigns [59]. Good results inferred from S-SEBI have been also reported by several other authors in different parts of the world [58,72,73].

6. Conclusions

In this paper, we have shown that the fraction of evaporation and latent heat flux are direct and simple indicators to monitor drought conditions of forest environments. Modeling the energy balance equation according to the S-SEBI approach shows that the surface parameters from satellite sensors, the albedo, vegetation index and surface temperature allow us to determine the heat flux latent (LE) simply and fast. The principal advantage of the proposed methodology is that the method requires only satellite data, so it is easy to implement and LE in areas without measurements can be estimated. However, the principal disadvantage of the methodology is that the studied images must contain extreme surface value temperatures.

In general, it can be said that the S-SEBI method works appropriately for high-resolution images, like Landsat ETM+ (NDVI pixel resolution of 30 m and T_0 of 60 m), and for heterogeneous and somewhat drier areas, like the ones studied here.

The results show that the sensible and latent heat fluxes are on the same order, with a slight surplus for the sensible heat. By analyzing the latent heat flux from the land cover, large spatial and temporal variations could be detected, although the simulated latent heat flux values should not be considered as being very accurate. However, by comparing different methods, a range of values close to the real ones could be estimated. The results obtained are in agreement with experimental data published in the literature. Unfortunately the validation test is mostly based on the comparison of results obtained with other methods, because we cannot access the ground surface flux for this study area .

The method provides estimates of air temperature close to reference measurements (RMSE = 0.78 ℃), but air temperature estimates are subject to local errors. Altitude is not the only factor affecting air temperature, but the advantage of this approach is that meteorological station data are not needed.

The sensitivity analysis demonstrated that errors in the determination of T_H and T_{LE} lines, and therefore in Λ, seem to affect the estimation of LE. This is the most critical point in the proposed methodology. However, the estimate of latent heat flux and other variables gave results comparable to those obtained in previous studies. Their comparison with other methods gave satisfactory results and validated the results in this study area. In addition, with a method such as S-SEBI evapotranspiration can be retrieved accurately. Given the simplicity of the models used in this study, our results are reasonable but could benefit from further studies.

The methodology adopted to map the energy balance terms with remote sensing data gave very promising results to monitor forest-cover in Algeria. If the input images of surface albedo and surface temperature show a lot of variation in surface conditions (wet/dry) and the atmospheric conditions are constant over the image, the S-SEBI model is a rather simple method to partition the surface energy balance terms without additional (field) data.

Finally, the application of S-SEBI does not require any *a priori* knowledge of the actual turbulent heat fluxes, indicating that S-SEBI is a credible and independent approach. Because of this, S-SEBI results may be used to validate and initialize hydrological, atmospheric and ecological models that usually require proper partitioning of the sensible and latent heat flux at different scales; in particular, to understand physical processes at different scales as well as the ability to obtain distributed physical information.

This method can also help monitor drought affected forests which will provide a better understanding of some crucial environmental issues such as fire risk, rain-wash or more generally soil protection and therefore lead to better management decisions in Algeria. Furthermore with this method a territorial investigation with more information about the spatial partition of surface energy can be performed. Finally, Satellite Earth observations will prove to be of utter importance for semi-arid regions, where few weather stations are in operation.

Acknowledgements

References and Notes

1. Peñuelas, J.; Filella, I.; Biel, C.; Serrano, L.; Save´, R. The reflectance at the 950–970 nm region as an indicator of plant water status. *Int. J. Remote Sens.* **1993**, *14*, 1887–1905.
2. Maki, M.; Ishiahra, M.; Tamura, M. Estimation of leaf water status to monitor the risk of forest fires by using remotely sensed data. *Remote Sens. Environ.* **2004**, *90*, 441–450.
3. Larcher, W. Physiological Plant Ecology. *Ecophysiology and Stress Physiology of Functional Groups*, 3rd ed.; Springer: New York, NY, USA, 1995; p. 528.
4. Jackson, R.D. Remote sensing of biotic and abiotic plant stress. *Annu. Rev. Phytopathol.* **1986**, *24*, 265–287.
5. Chuvieco, E.; Deshayes, M.; Stach, N.; Cocero, D.; Riaño, D. Short-Term Fire Risk: Foliage Moisture Content Estimation From Satellite Data. In *Remote Sensing of Large Wildfires in the*

European Mediterranean Basin; Chuvieco, E., Ed.; Alcala´ University press: Madrid, Spain, 1999; p. 228.

6. Desbois, N.; Pereira, J.M.; Beaudoin, A.; Chuvieco, E.; Vidal, A. Short Term Fire Risk Mapping Using Remote Sensing. In *A Review of Remote Sensing Methods for the Study of Large Wildland Fires*; Chuvieco, E., Ed.; Megafires: Alcala´, Spain, 1997; pp. 29–60.

7. Clothier, B.E.; Clawson, K.L.; Pinter, P.J.; Moran, M.S.; Reginato, R.J.; Jackson, R.D. Estimation of soil heat flux from net radiation during the growth of alfalfa. *Agr. Forest Meteorol.* **1986**, *37*, 319–329.

8. Desbois, N.; Vidal, A. La télédétection dans la prévision des incendies de forêts. *Ing énieries-EAT* **1**995, *1*, 21–29.

9. Jarvis, P.; James, G.; Landesburg, J. *Coniferous Forest* in *Vegetation and the Atmosphere*; Monteith, J.L., Ed.; Academic press: New York, NY, USA, 1976; Volume 2, pp. 171–236.

10. Gao, B.C.; Goetz, A.F.H. Retrieval of equivalent water thickness and information related to biochemical components of vegetation canopies from AVIRIS data. *Remote Sens. Environ.* **1995**, *52*, 155–162.

11. Gao, B.C. NDWI-A normalized difference water index for remote sensing of vegetation liquid water from space. *Remote Sens. Environ.* **1996**, *58*, 257−266.

12. Peñuelas, J.; Piñol, J.; Ogaya, R.; Filella, I. Estimation of plant water concentration by the reflectance Water Index WI (R900/R970). *Int. J. Remote Sens.* **1997**, *18*, 2869−2875.

13. Zarco-Tejada, P.J.; Rueda, C.A.; Ustin, S.L. Water content estimation in vegetation with MODIS reflectance data and model inversion methods. *Remote Sens.Environ.* **2003**, *85*, 109–124.

14. Ustin S.L.; Roberts, D.A.; Gamon, J.A.; Asner, G.P.; Green, R.O. Using imaging spectroscopy to study ecosystem processes and properties. *BioScience* **2004**, *54*, 523–534.

15. Peñuelas, J.; Filella, I.; Biel, C.; Serrano, L.; Savé, R. The reflectance at the 950–970 nm region as an indicator of plant water status. *Int. J. Remote Sens.* **1993**, *14*, 1887–1905.

16. Hamimed, A.; Mederbal, K.; Khaldi, A. Utilisation des données satellitaires TM de Landsat pour le suivi de l'état hydrique d'un couvet végétal dans les conditions semi-arides en Algérie. *T él él éection* **2001**, *2*, 29–38.

17. Ustin, S.L.; Roberts, D.A.; Jacquemoud, S.J.; Pinzón, S; Gardner, M.; Scheer, G.; Castaneda, C. M.; Palacios-Orueta, A. Estimating canopy water content of chaparral shrubs using optical methods. *Remote Sens. Environ.* **1998**, *65*, 280–291.

18. Chuvieco, E.; Cocero, D.; Riaño, D.; Martin, P.; Martınez-Vega, J.; Riva, J.; Perez, F. Combining NDVI and surface temperature for the estimation of live fuel moisture content in forest fire danger rating. *Remote Sens. Environ.* **2004**, *92*, 322–331.

19. Riaño, D.; Vaughan, P.; Zarco-Tejada, E.; Ustin, P.J. Estimation of fuel moisture content by inversion of radiative transfer models to simulate equivalent water thickness and dry matter content. Analysis at leaf and canopy level. *IEEE Trans. Geosci. Remote Sens.* **2005**, *43*, 819–826.

20. Petropoulos, G.; Carlson, T.N.; Wooster, M.J.; Islam, S. A review of Ts/VI remote sensing based methods for the retrieval of land surface energy fluxes and soil surface moisture. *Prog. Phys. Geo.* **2009**, *33*, 224–250.

21. Carlson, T.N.; Gillies, R.R.; Perry, E.M. A method to make use of thermal infrared temperature and NDVI measurements to infer surface soil water content and fractional vegetation cover. *Remote Sens. Rev.* **1994**, *9*, 161–173.

22. Moran, M.S.; Clarke, T.R.; Inoue, Y.; Vidal, A. Estimating crop water deficit using the relation between surface—air temperature and spectral vegetation index. *Remote Sens. Environ.* **1994**, *49*, 246–263.

23. Boegh, E.; Soegaard, H.; Hanan, N.; Kabat, P.; Lesch, L. A remote sensing study of the NDVI-Ts relationship and the transpiration from sparse vegetation in the Sahel based on highresolution satellite data. *Remote Sens. Environ.* **1999**, *69*, 224–240.

24. Moran, M.S. Thermal Infrared Measurement as an Indicator of Planet Ecosystem Health. *In Thermal Remote Sensing in Land Surface Processes*; Quattrochi, D.A., Luvall, J.C., Eds.; Tailor and Francis: London, 2004; pp. 257–282.

25. Luquet, D.; Vidal, A.; Dauzat, J.; Bégué, A.; Olioso, A.; Clouvel, P. Using direccional TIR measurements and 3D simulations to assess the limitations and opportunities of water stress indices. *Remote Sens. Environ.* **2004**, *90*, 53–62.

26. Batra, N.; Islam, S.; Venturini, V.; Bisht, G.; Jiang, L. Estimation and comparison of evapotranspiration from MODIS and AVHRR sensors for clear sky days over the Southern Great Plains. *Remote Sens. Environ.* **2006**, *103*, 1–15.

27. Menenti, M.; Bastiaanssen, W.G.M.; Van Eick, D.; Abl El Karim, M.A. Linear relationships between surface reflectance and temperature and their application to map evaporation of groundwater. *Adv. Space Res.* **1989**, *9*, 165–176.

28. Bastiaanssen, W.G.M.; Menenti, M.; Feddes, R.A.; Holtslag, A.A.M. A Remote sensing surface energy balance algorithm for land (SEBAL). 1. Formulation. *J. Hydrol.* **1998**, *213*, 198–212.

29. Kustas, W.P.; Norman, J.M. Use of remote sensing for evapotranspiration monitoring over land surfaces. *Hydrol. Sci. J.* **1996,** *41*, 495–516.

30. Su, Z.; Pelgrum, H.; Menenti, M. Aggregation effects of surface heterogeneity in land surface processes. *Hydrol. Earth Syst. Sci.* **1999**, *3*, 549–563.

31. Jackson, R.D.; Idso, S.B.; Reginato, R.J.; Pinter, P.J. Canopy temperature as a crop water stress indicator. *Water Resour. Res.* **1981**, *17*, 1133–1138.

32. Jackson, R.D.; Kustas, W.P.; Choudhury, B.J. A reexaminationof the crop water stress index. *Irrig. Sci.* **1988**, *9*, 309–317.

33. Choudhury, B.J.; Reginato, R.J.; Idso, S.B. An analysis of infrared temperature observations over wheat and calculation of latent heat flux. *Agr. Forest Meteorol.* **1986**, *37*, 75–88.

34. Kalma, J.D.; Jupp, D.L.B. Estimating evaporation from pasture using infrared thermometry: evaluation of a one-layer resistance model. *Agr. Forest Meteorol.* **1990**, *51*, 223–246.

35. Zhan, X.; Kustas, W.P.; Humes, K.S. An intercomparison study on models of sensible heat flux over partial canopy surfaces with remotely sensed surface temperature. *Remote Sens. Environ.* **1996**, *58*, 242–256.

36. Su, Z.; Schmugge, T.; Kustas, W.P.; Massman, W.J. An evaluation of two models for estimation of the roughness height for heat transfer between the land surface and the atmosphere. *J. Appl. Meteorol.* **2001**, *40*, 1933–1951.

37. Roerink, G.J.; Su, Z.; Menenti, M. S-SEBI: A simple remote sensing algorithm to estimate the surface energy balance. *Phys. Chem. Earth* **2000**, *25*, 147–157.

38. Verstraeten, W.W.; Veroustraete, F.; Feyen, J. Estimating evapotranspiration of european forests from noaa-imagery at satellite overpass time: Towards an operational processing chain for integrated optical and thermal sensor data products. *Remote Sens. Environ.* **2005**, *96*, 256–276.

39. Moran, M.S.; Jackson, R.D.; Raymond, L.H.; Gay, L.W.; Slater, P.N. Mapping surface energy balance components by combining Landsat Thematic Mapper and ground-based meteorological data. *Remote Sens. Environ.* **1989**, *30*, 77–87.

40. *Sourcebook on Remote Sensing and Biodiversity Indicators*; Strand, H., Höft, R., Strittholt, J., Horning, N., Miles, L., Fosnigh, E., Turner, W., Eds.; Secretariat of the Convention on Biological Diversity: Montreal, Canada, 2007; Technical series No. 32.

41. FIDA (International Fund for Agricultural Development). *Projet Pilote de Développement des Monts de Béni-Chougrane. Exploitation et Conservation des Ressources Naturelles.* FIDA press: Rome, Italy, 1991; Final report.

42. Souidi, Z. *Application de la Télédétection et des SIG Pour L'améNagement des Terres de Montagne: Cas des Monts de Béni-Chougrane (Mascara).* Thèse magister en science forestière, Faculté des sciences, Université de Tlemcen, Algeria, 2001; pp.66–103.

43. Berk, A.; Anderson, G.P.; Bernstein, L.S.; Acharya, P.K.; Dothe, H.; Matthew, M.W.; Adler-Golden, S.M.; Chetwynd, J.H.; Richtsmeier, S.C.; Pukall, B.; Allred, C.L.; Jeong, L.S.; Hoke, M.L. MODTRAN4 radiative transfer modeling for atmospheric correction. *Proc. SPIE* **1999**, *1*, 348–353.

44. Liang, S.; Shuey, C.; Russ, A.; Fang, H.; Chen, M.; Walthall, C.; Daughtry, C. Narrowband to Broadband Conversions of Land Surface Albedo: II. Validation. *Remote Sens. Environ.* **2002**, *84*, 25–41.

45. Rouse, J.; Deering, D. *Monitoring the Vernal Advancement and Retrogradation of Natural Vegetation*; Type III final report to the NASA/GSFC, Greenbelt, MD, USA, 1974.

46. Wukelic, G.E.; Gibbons D.E.; Martucci, L.M.; Foote, H.P. Radiometric calibration of Landsat Thematic Mapper thermal band. *Remote Sens. Environ.* **1989**, *28*, 339–347.

47. Van de Griend, A.A.; Owe, M. On the relationship between thermal emissivity and the normalized difference vegetation index for natural surfaces. *Int. J. Remote Sens.* **1993**, *14*, 1119–1131.

48. Barsi, J.A.; Barker, J.L.; Schott, J.R. An Atmospheric Correction Parameter Calculator for a Single Thermal Band Earth-Sensing Instrument. *Proc. IEEE Int.* **2003**, *5*, 3014–3016.

49. Irish, R.R. *Landsat 7 science data user's handbook*. Report 430-15-01-003-0; National Aeronautics and Space Administration, 2000; [Online] http://ltpwww.gsfc.nasa.gov/IAS/handbook/handbook_toc.html(accessed on 19 October 2009).

50. Mauser, W.; Stephan, S. Modelling the spatial distribution of evapotranspiration on different scales using remote sensing data. *J. Hydrol.* **1998**, *212–213*, 250–267.

51. Menenti, M.; Choudhury, B.J. Parameterization of land surface evapotranspiration using a location dependent potential evapotranspiration and surface temperature range. In *Proceedings of Exchange Processes at the Land Surface for a Range of Space and Time Scales*; Bolle, H.J., Feddes, R.A., Kalma, J.D., Eds.; IAHS: Wallingford, UK, 1993; Volume 212, pp. 561–568.

52. Engman, E.T.; Gurney, R.J. *Remote Sensing in Hydrology*; Chapman and Hall: London, UK, 1991.

53. Duffie, J.A.; Beckman, W.A. *Solar Engineering of Thermal Process*, 2nd ed.; John Wiley & Sons: New York, NY, USA, 1991.

54. Brutsaert, W. On a derivable formula for longwave radiation from clear skies. *Water Resour. Res.* **1975**, *11*, 742–744.

55. Crago R.D. Conservation and variability of the evaporative fraction during the daytime. *J. Hydrol.* **2000**, *180*, 173–194.

56. Shuttleworth, W.J.; Gurney, R.J.; Hsu, A.Y.; Ormsby, J.P. *FIFE: The Variation in Energy Partitioning at Surface Flux Sites*; IAHS Red Book: Wallingford, UK, 1989; Series No. 186, pp. 67–74.

57. Bastiaanssen, W.G.M.; Pelgrum, H.; Meneti, M.; Feddes, R.A. Estimation of Surface Resistance and Priestley-Taylor α Parameter at Different Scales. In *Scaling Up in Hydrology Using Remote Sensing*; Stewart, J.B., Engman, E.T., Feddes, R.A., Kerr, Y., Eds.; Institute of Hydrology: Wallingford, UK, 1996; pp. 93–111.

58. Sobrino, J.A.; Gómez, M.; Jiménez-Muñoz, J.C.; Oliosob, A.; Chehbouni, G. A simple algorithm to estimate evapotranspiration from DAIS data: Application to the DAISEX campaigns. *J. Hydrol.* **2005**, *315*, 117–125.

59. Jia, L. *Modeling Heat Exchanges at the Land-Atmosphere Interface Using Multi-Angular Thermal Infrared Measurements*; Wageningen University: Wageningen, Netherlands, 2004.

60. Jaeger, L.; Gessler A.; Kastendeuch, P.; Kodama, N.; Lehner, I.; Najjar, G.; Parlow, E.; Paul, P.; Rennenberg, H.; Post, J.; Viville, D.; Vogt, R.; Zygmuntowski, M. Impacts des changements climatiques sur le comportement de la végétation dans le fossé de Rhénan. *Ann. assoc. climatol.* **2005**, *2*, 137–149.

61. Prospert-Laget, V. A satellite index of risk of forest fire occurrence in summer in the mediterranean area. *Int. J. Wildland Fire* **1998**, *8*, 173–182.

62. Bougeault, P.; Noilhan, J.; Lacarere, P.; Mascart, P. An experiment with an advanced surface parameterization in a meso-beta-scale model. Part I: Implementation. *Monthly Weather Rev.* **1991**, *119*, 2358–2373.

63. Bastiaanssen, W.G.M.; Van Der Wall, T.; Visser T.N.M. Diagnosis of regional evaporation by remote sensing to support irrigation performance assessment. *Irrig. Drain. Syst*. **1996**, *10*, 1–23.

64. Guyot, G. *Climatologie de l'environnement*; Dunod: Paris, France, 1999.

65. Wilegepolage, K. *Estimation of Spatial and Temporal Distribution of Evapotranspiration by Satellite Remote Sensing*; ITC press: Enschede, Netherlands, 2005.

66. Jiang, L.; Islam, S. A methodology for estimation of surface evapotranspiration over large areas using remote sensing observations. *Geophys. Res. Lett.* **1999**, *26*, 2773–2776.

67. Jiang, L.; Islam, S. An intercomparison of regional latent heat flux estimation using remote sensing data. *Int. J. Remote Sens.* **2003**, *24*, 2221–2236.

68. Stisen, S.; Sandholt, I.; Nørgaard, A.; Fensholt, R.; Jensen, K.H. Combining the triangle method with thermal inertia to estimate regional evapotranspiration – Applied to MSG/SEVIRI data in the Senegal River basin. *Remote Sens. Environ.* **2008**, *112*, 1242–1255.

69. Carlson, T. An overview of the "Triangle Method" for estimating surface evapotranspiration and soil moisture from satellite imagery. *Sensors* **2007**, *7*, 1612–1629.

70. Gomez, M.; Olioso, A.; Sobrino, J.A.; Jacob, F. Retrieval of Evapotranspiration Over the Alpilles/ReSeDA Experimental Site Using Airborne POLDER Sensor and a Thermal Camera. *Remote Sens. Environ.* **2005**, *96*, 399–408.

71. Were, A.; Villagarcia, L.; Domingo, F.; Alados-Arboledas, L.; Puigdefabregas, J. Analysis of effective resistance calculation methods and their effect on modelling evapotranspiration in two different patches of vegetation in semi-arid se spain. *HESSD* **2007**, *4*, 1–44.

72. Sobrino, J.A.; Gómez, M.; Jiménez-Muñoz, J.C.; Olioso, A. Application of a simple algorithm to estimate the daily evapotranspiration from NOAA-AVHRR images for the Iberian Peninsula. *Remote Sens. Environ.* **2007**, *110*, 139–148.

73. Fan, L.; Liu, S.; Bernhofer, C.; Liu, H.; Berger, F.H. Regional land surface energy fluxes by satellite remote sensing in the Upper Xilin River Watershed (Inner Mongolia, China). *Theor. Appl. Climatol.* **2007**, *88*, 231–245.